Journal of Hazardous Materials 213–214 (2012) 184–192

Contents lists available at SciVerse ScienceDirect

Journal of Hazardous Materials

journal homepage: www.elsevier.com/locate/jhazmat

Effect of precursor and preparation method on manganese based activated carbon sorbents for removing H_2S from hot coal gas

Jiancheng Wang[a], Biao Qiu[a], Lina Han[a,b], Gang Feng[c], Yongfeng Hu[d], Liping Chang[a], Weiren Bao[a,*]

[a] Key Laboratory of Coal Science and Technology, Taiyuan University of Technology, Ministry of Education and Shanxi Province, Taiyuan 030024, PR China
[b] College of Materials Science and Engineering, Taiyuan University of Technology, Taiyuan 030024, PR China
[c] Shanghai Research Institute of Petrochemical Technology SINOPEC, Shanghai 201208, PR China
[d] Canadian Light Source, 101 Perimeter Road, Saskatoon, SK, Canada S7N 0X4

ARTICLE INFO

Article history:
Received 10 August 2011
Received in revised form 20 January 2012
Accepted 23 January 2012
Available online 1 February 2012

Keywords:
Metal oxide/AC sorbent
Supercritical water impregnation
Pore volume impregnation
Precursor
Desulfulrization

ABSTRACT

Activated carbon (AC) supported manganese oxide sorbents were prepared by the supercritical water impregnation (SCWI) using two different precursor of $Mn(NO_3)_2$ (SCW(N)) and $Mn(Ac)_2{\cdot}4H_2O$ (SCW(A)). Their capacities of removing H_2S from coal gas were evaluated and compared to the sorbents prepared by the pore volume impregnation (PVI) method. The structure and composition of different sorbents were characterized by XRD, SEM, TEM, XPS and XANES techniques. It is found that the precursor of active component plays the crucial role and SCW(N) sorbents show much better sulfidation performance than the SCW(A) sorbents. This is because the Mn_3O_4 active phase of the SCW(N) sorbents are well dispersed on the AC support, while the Mn_2SiO_4-like species in the SCW(A) sorbent can be formed and seriously aggregated. The SCW(N) sorbents with 2.80% and 5.60% manganese are favorable for the sulfidation reaction, since the Mn species are better dispersed on the SCW(N) sorbents than those on the PV(N) sorbents and results in the better sulfidation performance of the SCW(N) sorbents. As the Mn content increases to 11.20%, the metal oxide particles on AC supports aggregate seriously, which leads to poorer sulfidation performance of the SCW(N)11.20% sorbents than that of the PV(N)11.20% sorbents.

1. Introduction

Coal-derived fuel gas contains several sulfur gases (nearly 90% is H_2S), which could corrode equipments, poison catalysts and seriously endanger the environment and human health [1,2]. The removal of H_2S from coal gas is an important step to improve the cleaning use of coal. The optimal temperature for hot gas cleaning is subject to debate [3]. Considering the efficiency of heat usage and the adapted operation in practice, some researchers focused on the development of the efficient desulfurization at medium temperature range (250–450 °C), which is of importance to promote the coal gas cleaning technology and improve the efficiency of coal utilization [3]. Many sorbents, such as zinc oxide, iron oxide, manganese oxide, copper oxide, calcium oxide, zinc titanate and zinc ferrite, were used for the removal of H_2S from hot coal gas [4–10].

The manganese oxides, both supported and unsupported, have attracted great attention as catalytically active components in a variety of catalytic reactions, e.g., the low-temperature selective catalytic reduction of NO with NH_3 [11,12]; the oxidation of alcohol [13,14]. Moreover, manganese oxides have been employed for the removal of hydrogen sulfide [15]. Various active manganese state and dispersion of particles can be obtained using different precursors and preparation methods, which influence the activity of the catalysts. Many researchers found that the calcination temperature determined the final oxidation state of the supported manganese [16–18]. It was reported that MnO_2 on alumina support is mainly formed below 427 °C and Mn_2O_3 formed at 627 °C [19,20]. Highly dispersed activated carbon supported manganese oxides (Mn loading of ca. 5 wt.%) can be obtained at the modest pretreatment temperatures by conventional wet impregnation method using manganese nitrate as precursor, whereas the large amount of Mn loading will result in the aggregated MnO_x crystalline [21].

As a generalized crystallization method for the production of metal oxide particles, supercritical water techniques applied to the production of nanoparticles and nanostructured materials are highlighted [22–27]. The use of supercritical water impregnation (SCWI) in preparing sorbent appears to be a promising method, which could produce uniform in size and chemical composition stabilized particles by optimizing the reaction temperature and pressure. In addition, the use of water as reaction medium other than toxic or noxious solvents simplifies the process and post-treatments, such as pollutants recovery, calcination and drying [27–31]. Our recent

* Corresponding author. Tel.: +86 351 6010482; fax: +86 351 6010482.
E-mail addresses: jc_wang2008@yahoo.com (J. Wang), baoweiren@tyut.edu.cn (W. Bao).

0304-3894/$ – see front matter © 2012 Elsevier B.V. All rights reserved.
doi:10.1016/j.jhazmat.2012.01.080

work found that the desulfurization activity of the sorbent, the loading amounts of metal oxide, the dispersion of particles and the micropore structure properties of the sorbent are controlled by the preparation temperature, impregnation time, and concentration of the precursor solution. The optimal SCWI conditions for preparing Mn/AC sorbents are 380 °C preparation temperature and 30 min impregnation time [32].

In the present work, the sorbents were prepared by depositing the Mn oxide particles onto the activated carbon (AC) using SCWI method with different Mn precursor solutions. For comparison, the sorbent was also prepared by pore volume impregnation (PVI) method. The desulfurization activities of the sorbents were investigated in simulated coal-derived gas. The X-ray diffraction (XRD), scanning electron microscope (SEM), transmission electron microscope (TEM), X-ray photoelectron spectroscopy (XPS) and X-ray absorption near edge structure (XANES) were employed to explain the different reaction activities of the sorbents obtained with different precursor and preparation method.

2. Experimental

2.1. Preparation of sorbent

The AC with the particle sizes of 8–10 mesh, which was made from coal, was used as supports. Table 1 shows the proximate and ash analyses of the AC, which indicates there are SiO_2, Al_2O_3 and CaO, MgO, Fe_2O_3, etc. in the sample.

A series of sorbents were prepared in a 300 mL stainless-steel autoclave, equipped with a pressure gauge and a thermocouple, using SCWI method. The reactor was heated using an external heating furnace with a temperature controller. Precursor solutions were prepared by dissolving a certain amount of $Mn(NO_3)_2$ or $Mn(Ac)_2{\cdot}4H_2O$ in 100 mL deionized water. The precursor solution and 20 g AC were added to the stainless-steel autoclave for each run. The autoclave was heated to 380 °C and maintained for 30 min as we had been reported elsewhere [32]. After that, the autoclave was cooled to 200 °C, the pressure valve was opened and the gas–liquid–solid products were quickly separated. The solid samples were directly used as the sorbents for the removal of H_2S from simulated hot coal gas. The samples were named as SCW(N)*x*% and SCW(A)*x*%, where (N) and (A) represent the precursor of the manganese nitrate and manganese acetate, and '*x*%' represents the mass ratio of the metal Mn to Mn/AC in the 100 mL solution. The used (after the sulfidation process) samples are named as S-SCW(N)*x*% and S-SCW(A)*x*%, respectively.

The $Mn(NO_3)_2$ solution was also used to prepare the sorbents using PVI method. The sorbents were subsequently dried at 120 °C for 2 h and then calcined in N_2 gas at 500 °C for 4 h. PV(N)*x*% was used to represent the sorbent prepared by PVI method. To keep in consistent with the $Mn(NO_3)_2$ solution in the sorbent prepared by SCWI method, where '*x*%' was set as 2.80%, 5.60%, 11.2%, so "*x*" can not reflect the real content of Mn in the Mn/AC. The actual Mn content in sorbent will be determined by inductively coupled plasma-atomic emission spectrometry (ICP-AES). The used (after the sulfidation process) samples are named as S-PV(N)*x*%.

2.2. Sulfidation test

The sulfidation tests of the MnO_x/AC sorbents were carried out at atmospheric pressure using a fixed-bed flow microreactor. The typical reactant gas mixture consists of 52 vol% H_2, 33 vol% CO, 500 ppm H_2S and N_2 balance gas. All the sulfidation tests were carried out at 350 °C with a space velocity of 2000 h^{-1}. The concentration of H_2S was analyzed using the gas chromatographs (GC950, Shanghai Haixin Chromatographic Instrument Co., Ltd.) equipped with a flame photometry detector (FPD, GDX-303). The test was stopped when the concentration of H_2S in outlet gas was higher than 100 ppm and the desulfurization efficiency was less than 80%. The sulfur capacity is the mass of sulfur adsorbed by 100 g of fresh sorbent. The theoretical sulfur capacity was calculated on the basis of the assumption that all the Mn content in the sorbent exists in the form of Mn_3O_4 and the Mn_3O_4 completely transforms into Mn_3S_4 during the reaction. The computation details for the desulfurization efficiency, the sulfur capacity and the use rate of the sorbent have been reported in our previous work [33], the data obtained in this work are calculated by referring it.

The sorbent regeneration was carried out at the same microreactor. The typical reactant gas mixture contains 1.2 vol% O_2, 0.5 vol% NH_3, 15% H_2O and N_2 balance gas. All the tests were done at 520 °C with a space velocity of 2000 h^{-1}. The concentration of H_2S and SO_2 were analyzed using the gas chromatographs and flue gas analyzers (British, Kane-9106). The test was stopped when the concentrations of H_2S and SO_2 in outlet gas were more/less than 10 ppm and 20 ppm, respectively.

2.3. Characterization of sorbent

X-ray diffraction (XRD) was employed to investigate the crystal structures of the sorbents. The instrument was equipped with a Rigaku D/max2500 diffractormeter, a graphite monochromator and Cu Kα radiation sources ($\lambda = 0.154056$ nm), and the tube voltage and current are 40 kV and 100 mA, respectively. The scan rate was 8°/min for 2θ values of 20–75°.

The metal content of the samples was analyzed with ICP-AES. The MnO_x/AC sorbents were grinded to about 200 mesh, and calcinated at 500 °C in air. The ash obtained was digested using the mixture of nitric acid and hydrochloric acid.

The pore structure was determined via nitrogen adsorption at 77 K using a Micromeritics ASAP2000 analyzer. The surface area and micropore volumes were calculated using the Brunauer–Emmett–Teller (BET) equation.

The surface morphology was observed by a scanning electron microscopy (JSM-6700F, JEOL, Japan). The samples were covered with a thin gold layer and the accelerating voltage was 10 kV. The crystalline phases of samples were measured by transmission electron microscopy (TEM) at the room temperature with a JEOL2100f microscope operating at 200 kV.

X-ray photoelectron spectroscopy (XPS) surface analysis was conducted for determining the surface concentration and binding energy of Mn $2p_{3/2}$, using an ESCALAB 250 spectrometer (VG Scientific Ltd., UK) equipped with an monochromated Al Kα ($h\upsilon = 1486.6$ eV, 150 W). The spectrometer was calibrated using the photoemission lines of Au (Au $4f_{7/2} = 83.95$ eV), Ag (Ag $3d_{5/2} = 368.2$ eV) and Cu (Cu $2p_{3/2} = 932.62$ eV). No smoothing routine of data was applied to analyze the results.

The X-ray absorption spectroscopy (XAS) measurement of samples before and after sulfidation was performed at the Canadian Light Source, using the Soft X-ray Micro characterization Beam line (SXRMB). Si(1 1 1) double crystal monochromotor was used, giving an energy resolving power of 10,000 eV [34] The sample was mounted using double-sided, conducting carbon tape, and loaded into a vacuum chamber (base pressure of 1×10^{-8} torr). Mn and S K-edge XAS spectra were recorded in the surface sensitive total electron yield (TEY) by monitoring the drain sample current, and the bulk sensitive fluorescence yield (FLY) with a silicon(Li) drifted detector. The energy scale was calibrated using the Ar K-edge in the upstream ion chamber and a sulfate peak at 2481.6 eV. The accuracy of energies reported here is 0.1 eV. Representative Mn oxide or sulfate compounds included manganese monoxide (MnO), manganese(II, III) oxide (Mn_3O_4), manganese sesquioxide (Mn_2O_3),

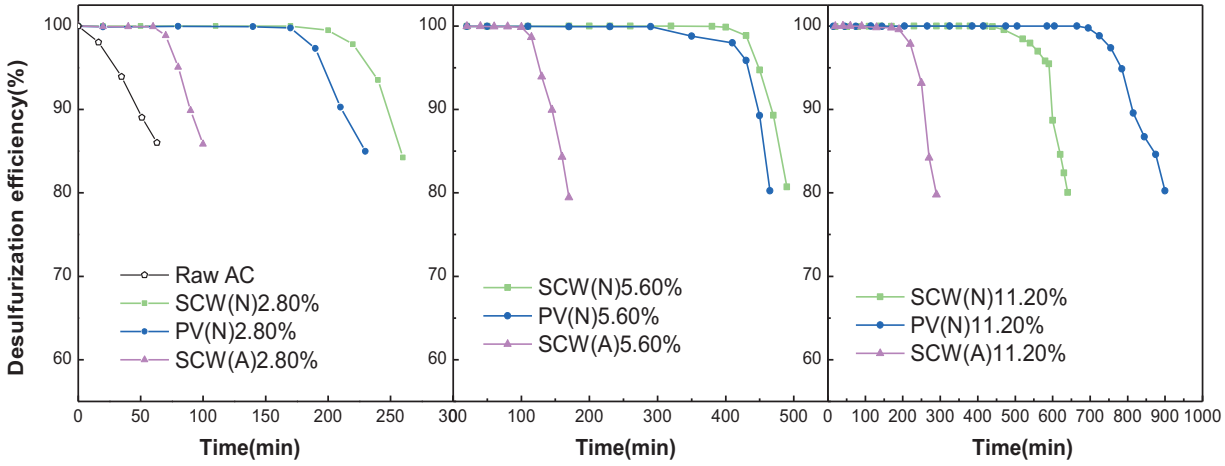

Fig. 1. Desulfurization efficiency of sorbents prepared from different concentration precursor solution and different method.

manganese dioxide (MnO_2), manganese(II) sulfide (MnS). All the reference compounds were obtained from Aldrich (>97%).

3. Results and discussions

3.1. Effect of precursor and preparation method on the desulfurization activity of sorbent

In order to investigate the effect of the precursor on the desulfurization activity of the sorbent, a series of sorbents (SCW(N)2.80%, 5.60%, 11.2%; SCW(A)2.80%, 5.60%, 11.2%; PV(N)2.80%, 5.60%, 11.2%) were prepared with various manganese oxide contents ranging in 2.80–11.20%. The Mn contents in sorbents and the physical parameters of the prepared sorbents are shown in Table 2. The metal loading contents of manganese are lower in SCW(N) and PV(N) samples compared to that of SCW(A) when Mn concentration is lower (2.80%), while there is no obvious difference in the metal loading contents for all samples when Mn concentrations are higher (5.6% and 11.20%).

The sulfidation breakthrough curves of the prepared samples and the raw AC are shown in Fig. 1. The desulfurization performance of AC is very poor and the breakthrough time is only 70 min. Moreover, about 50 ppm COS was detected in the outlet gas for the raw AC sorbent. For the reference, the content of COS of the MnO_x/AC sorbent is lower than 0.5 ppm. COS is mainly the product of reaction between H_2S and CO, which is dominated by H_2S content in ambient gases. It is obvious that much better desulfurization performance was achieved by MnO_x/AC.

It is clear from Fig. 1 and Table 2 that desulfurization activities of the Mn/AC sorbents obtained using different methods or different precursor solutions are different. The breakthrough time and sulfur capacity of the SCW(N) 2.80, 5.60 and 11.20% sorbents are 270, 490 and 640 min and 1.51, 2.97, 3.91 g S/100 g sorbent, respectively; 110, 170, 290 min and 0.54, 0.91, 1.66 g S/100 g sorbent for the SCW(A)2.80, 5.60 and 11.20% sorbents, respectively; and 250, 475, 900 min and 1.43, 2.83, 5.41 g S/100 g sorbent for the PV(N) 2.80, 5.60, 11.20% sorbents, respectively. This indicates that the composition of precursor influences the desulfurization activity of sorbents prepared using SCWI, and the desulfurization precision and desulfurization capacities of sorbents prepared from $Mn(NO_3)_2$ are much better than those prepared from $Mn(Ac)_2{\cdot}4H_2O$. It is also found that the performance of PV(N) samples shows similar performance to those of SCW(N) samples. It should be noted that the usage rates of active component, which were defined as the ratio of actual and theoretical sulfur capacities [33], in SCW(N)*x*% sorbents at lower loadings (2.80% and 5.60%) are very high and slightly better than those of PV(N) samples (Table 2). While the usage rate of active component at higher metal loading decreases to 51.23% for the SCW(N)11.20% sample, which is inferior to 70.90% of PV(N)11.20%. It shows that the preparation methods and precursor solutions all have obvious effects on the desulfurization activity of sorbents.

3.2. Main factors influencing the desulfurization activity of sorbent

As we know, the activities of supported sorbents/catalysts depend on many factors, such as the crystal forms, the dispersion and the valence state of the metal active components on the support and so on. In order to identify and understand the key factors that contribute to the performance of the prepared samples, N_2 adsorption–desorption, XRD, SEM, TEM, XPS and XANES were employed to investigate the fresh and used samples.

3.2.1. N_2 adsorption–desorption

Fig. 2 shows the adsorption–desorption isotherms of the AC and SCW(N) sorbents. On the basis of IUPAC classification, all samples display type IV sorption isotherms with hysteresis loops at $P/P_0 = (0.40–1.0)$. This suggests that there are secondary mesopores in these materials [35]. As shown in Table 2, there is no obvious difference in surface area and pore diameter for the SCW(N), SCW(A) and the PV(N) samples at low concentration of precursor solution (2.80%). But at higher concentrations, the surface areas of the SCW(N)11.20%, SCW(A)11.20% are higher than those of PV(N)11.20%. This is probably because the SCWI could

Table 1
Proximate and ash analyses of activated carbon (AC).

Proximate analysis (wt%)			Ash composition (wt%)						
M_{ad}	A_{ar}	V_{ar}	SiO_2	Al_2O_3	Fe_2O_3	TiO_2	CaO	MgO	The others[a]
10.43	12.01	2.33	33.02	16.50	8.34	0.77	14.91	5.06	21.40%

Note: ad, air dried; ar, as received; a, by difference.

Table 2
Physical parameters of sorbents prepared using different concentration precursor solutions and different methods.

Sorbents	Metal content (%)	Sulfur capacity (g S/100 g)	Mn utilization (%)	Surface area (m^2/g)	Pore diameter (nm)
SCW(N) 2.80%	2.02	1.51	90.96	968.3	2.273
SCW(A) 2.80%	3.04	0.54	22.46	956.7	2.249
PV(N) 2.80%	2.00	1.43	86.14	960.7	2.280
SCW(N) 5.60%	4.45	2.97	80.93	–	–
SCW(A) 5.60%	4.83	0.91	26.47	–	–
PV(N) 5.60%	4.40	2.83	77.11	–	–
SCW(N) 11.20%	9.26	3.91	51.23	913.9	2.229
SCW(A) 11.20%	9.16	1.66	21.99	904.8	2.221
PV(N) 11.20%	9.20	5.41	70.90	835.6	2.200
AC	0.00	0.30	–	999.8	2.255

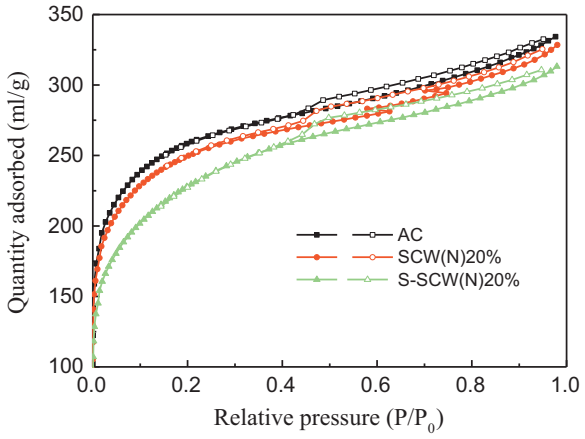

Fig. 2. N_2 adsorption–desorption isotherms of AC, fresh and used SCW(N)11.20% sorbents.

enlarge the pore of AC and increase BET surface area, however, the impregnation with high concentration precursor usually blocks the pore of the support and decreases its BET surface area. These two effects were neutralized for the SCWI sorbents, yet obvious reduction occurred for the PVI sorbents. The correlation between the desulfurization performance and pore structure of the sorbents shows that the surface area and pore diameter have no obvious influence on the desulfurization activity and capacity. The surface area of the Mn/AC is not a major factor on the desulfurization activity.

3.2.2. XRD

Fig. 3 shows the XRD patterns of the raw AC and MnO_x/AC sorbents prepared with different precursors and preparation methods before and after sulfidation. The SCW(A) sorbents show the presence of and Mn_2SiO_4-like species [36,37] which was probably produced by the reaction of Mn salt solution with the Si species of the AC (shown in Table 1) during SCWI processing. The strong patterns Mn_2SiO_4-like species of the SCW(A)2.80% results in its low desulfurization activity, since the Mn_2SiO_4-like species is very stable and were not involved with the sulfidation reaction, as indicated by the XRD data that there is still strong pattern of Mn_2SiO_4-like species after the sulfidation reaction (Fig. 3(b)). The same trend was also observed for the SCW(A)11.20% sample.

Only diffractions peaks ascribed to Mn_3O_4 are observed for the SCW(N) sorbents. The diffraction peak assigned to crystalline MnO is observed for all the sorbents prepared by PVI and the weak diffraction peaks of MnO becomes more noticeable as the Mn content increases from 2.80% to 11.20%. The characteristic patterns of MnS in the S-SCW(N)11.20% are stronger than that of the used PV(N)11.20% sorbent, which indicates the MnS are better dispersed in PV(N)11.20% than in the SCW(N)11.20%. It indicates that better dispersion of active metal component in PV(N)11.20% results in the better activity of H_2S removal than that of SCW(N)11.20%. On the other hands, the diffraction peaks corresponding to MnS are not detected on the AC and S-SCW(A) samples due to the their poor sulfidation performance with very little containing-S components produced. XRD peaks have not the obvious changes for AC support before and after sulfidation reaction and no sulfide is detected in used AC. These results show that the desulfurization mechanism of AC is different from MnO_x loaded on AC and the metal oxides

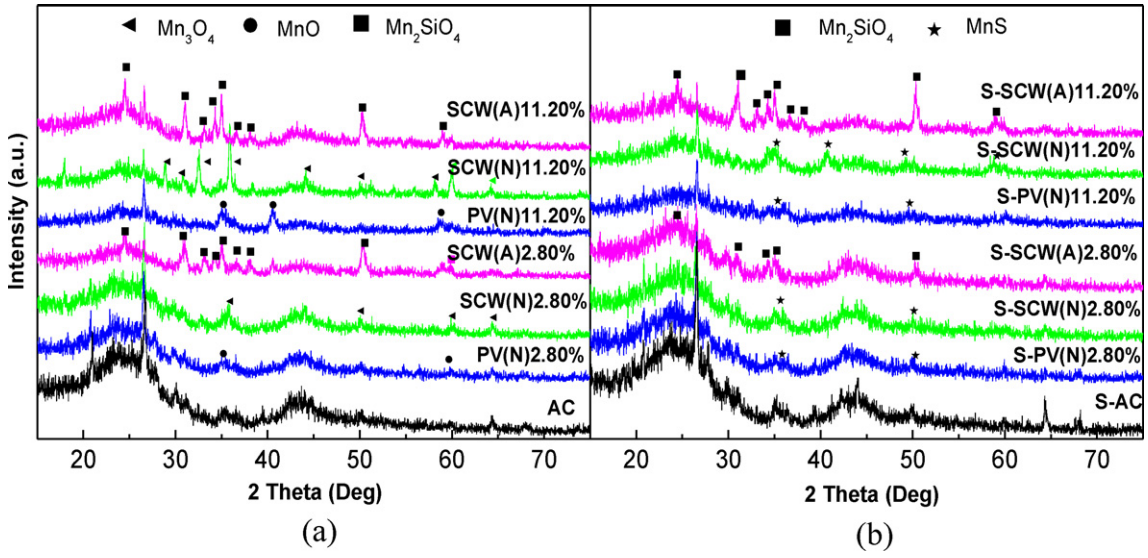

Fig. 3. XRD patterns of sorbents prepared from different concentration precursor solution and different method before (a) and after (b) sulfidation.

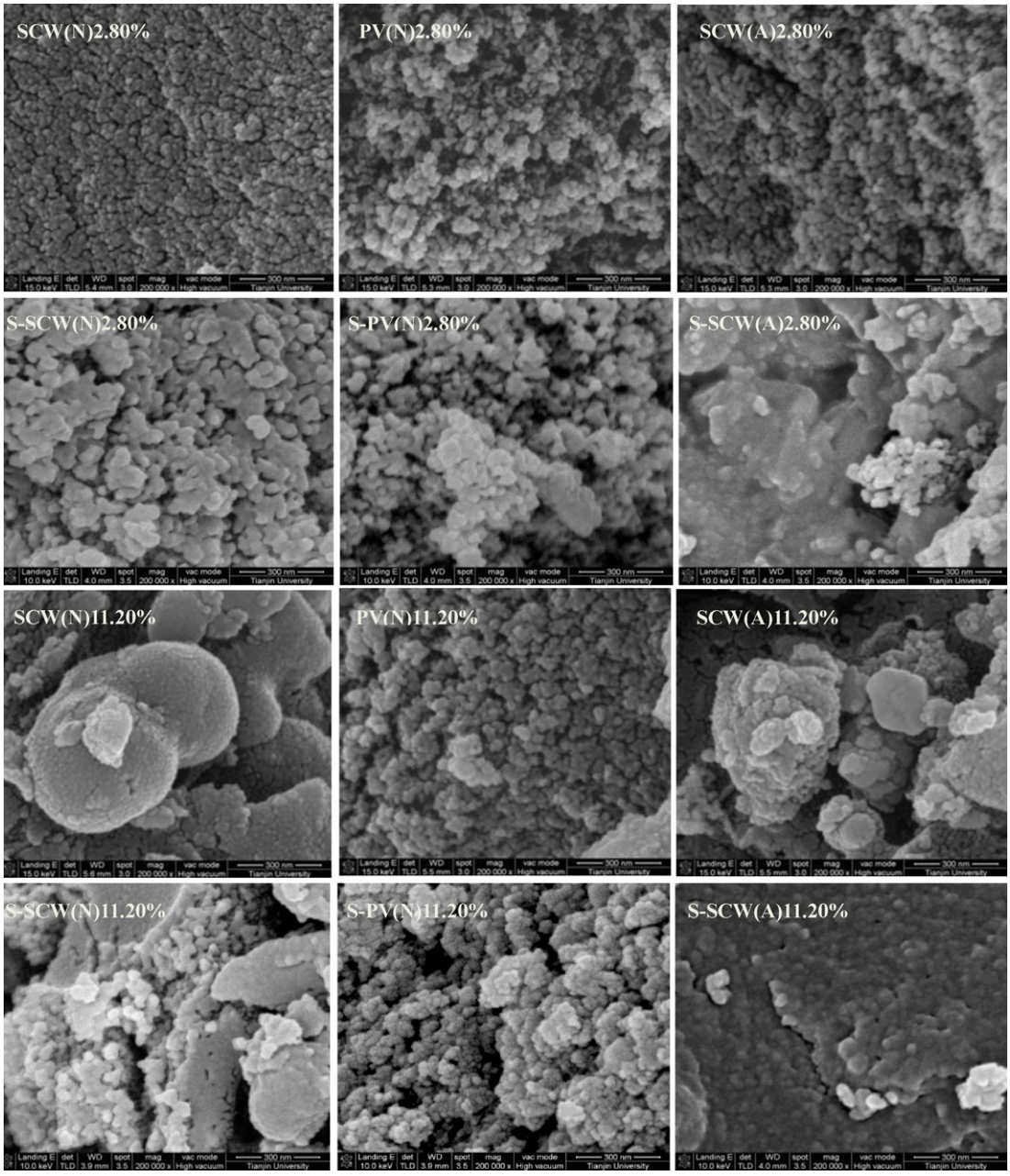

Fig. 4. SEM images of fresh and used sorbents prepared from different concentration precursor solution and different method.

detected in the ash of AC (shown in Table 1) have the small effect for the sulfidation reaction of MnO_x/AC sorbent.

3.2.3. SEM and TEM

It is recognized that the smaller crystal size results in the more active sites which are favorable for the sulfidation reaction [38]. The dispersion and mean size of the fresh and used sorbents were investigated using SEM and TEM. Fig. 4 shows the representative SEM images of the SCWI and PVI sorbents before and after sulfidation. The SEM image shows that the SCW(N)2.80% sorbent has small and uniform size and the active Mn species are well dispersed on the surface of support. While some of the particles agglomerates for the SCW(A)2.80% and PV(N)2.80% sorbents and the particles sizes are larger than those of SCW(N)2.80% sorbent. The particles agglomerate apparently and large size particles are formed in SCW(N)11.20% and SCW(A)11.20% sorbents. In contrast, only a few particle aggregations are observed for the PV(N)11.20% sorbents compared with the PV(N)2.80% sorbent.

The TEM images of the sorbents are presented in Fig. 5. It is found that the fine particles of crystalline phase of the SCW(N)2.80%, SCW(A)2.80% and PV(N)2.80% sorbent are of 20–40, 50–100 and 25–80 nm, respectively, vs. 30–200, 60–200 and 30–100 nm for the SCW(N)11.20%, SCW(A)11.20% and PV(N)11.20% sorbents. These particle diameters are smaller than that results reported by Choi et al. [39]. Since the manganese components of the SCW(A) sorbent seriously agglomerate and was poorly dispersed on the support, it results in the poor desulphurization activity of the SCW(A) sorbents. Manganese oxide on the SCW(N)2.80% sorbents were dispersed better than on the PV(N)2.80% sorbents. While, the manganese oxide of SCW(N)11.20% aggregates more seriously than the PV(N)11.20% sorbents. This indicates high dispersion and fine particles of the active component results in high activity of

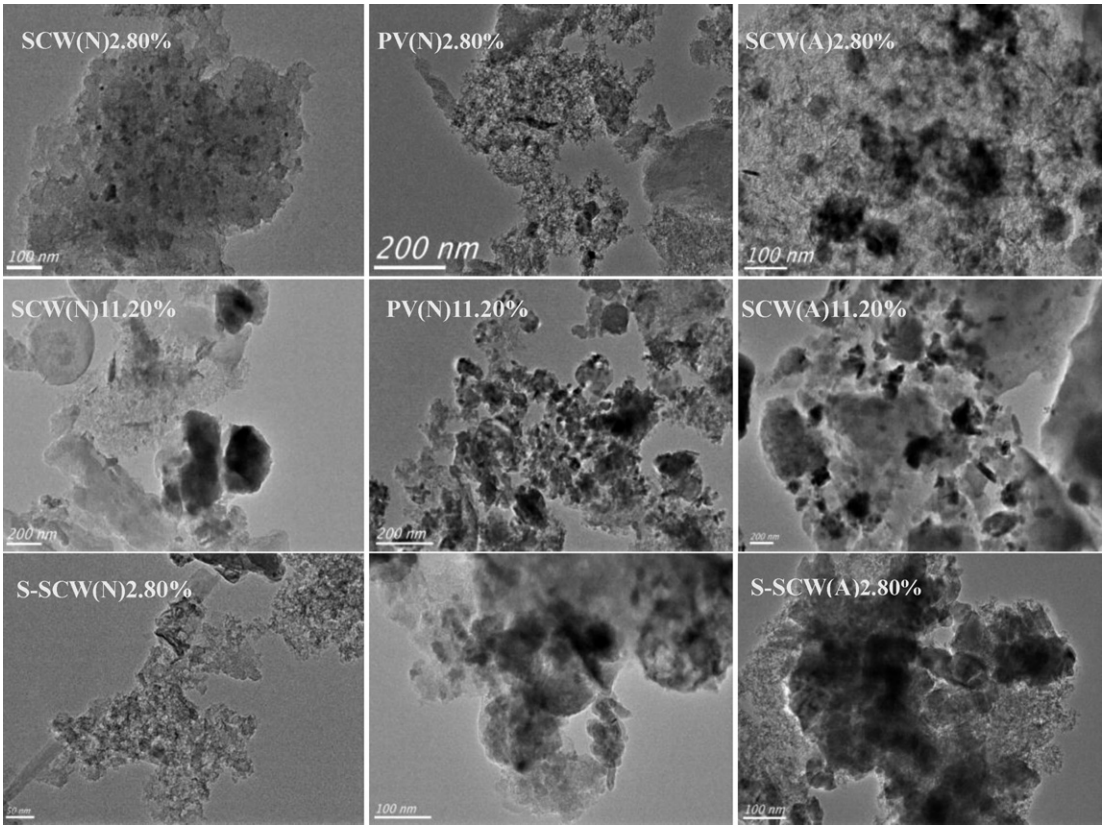

Fig. 5. TEM images of fresh and used sorbents prepared from different concentration precursor solution and different method.

desulphurization and it is consistent with the desulfurization results of the sorbents obtained from different preparation methods.

The SEM image in Fig. 4 shows that particle sizes of S-PV(N)2.80% and S-SCW(N)2.80% sorbents were slightly larger than the fresh sorbents. It has been reported that The 5Fe–15Mn–40Zn–40Ti–O solid after sulfidation and regeneration consists of large aggregates of different sizes [40] and the same results also can be found in the literature [39]. While, the particles of S-SCW(A)2.80% sorbent agglomerated clearly. It is also found that particles of the S-SCW(A)11.20% is agglomerated more seriously than those of S-SCW(N)11.20%, which was also more serious than those of S-PV(N)11.20%. The TEM image of used sorbents (Fig. 5) shows that the manganese species of S-SCW(N)2.80% sorbent exhibits the best dispersion, while the manganese species of S-PV(N)2.80% appear as relatively large particles, and the serious agglomeration of manganese species can be observed in S-SCW(A)2.80% sample. The aggregation degree of active components after sulfidation process is in agreement with the desulfurization performance.

3.2.4. XPS

The chemical states of the surface Mn species for the sorbents before and after the sulfidation process were investigated using XPS and the results are presented in Fig. 6. It is found that different sorbents exhibit different binding energies of $Mn2p_{3/2}$. The broad binding energies of $Mn2p_{3/2}$ in SCW(N)11.20% can be resolved into 640.5 eV, and 641.5 eV which can be assigned to Mn^{2+} and Mn^{3+}, respectively [18,19]. Tang et al. [21] reported that Mn_3O_4 has a normal spinel structure with Mn^{2+} ions in tetrahedral sites and Mn^{3+} ions in tetragonally distorted octahedral sites. The XPS and XRD results indicate that the Mn_3O_4 on the surface layer of sorbent exists in the form of $MnO{\cdot}Mn_2O_3$. The broad binding energies of around 640.7 eV for the Mn $2p_{3/2}$ in SCW(A)11.20% are assigned to the Mn species in Mn_2SiO_4-like species [41], which also agree well with the XRD results. The binding energies of the Mn $2p_{3/2}$ and $Mn2p_{1/2}$ in PV(N)11.20% sorbents are 641.7 and 653 eV, respectively, which are assigned to Mn^{2+} and Mn^{3+}.

The three sorbents after the sulfidation process show different spectral features. The binding energies of 639.9 eV is assigned to MnS. The binding energies of SCW(N)11.20% and PV(N)11.20% sorbents change dramatically after the sulfidation process and Mn in the form MnS on their surface are detected, it suggests that quite a lot Mn components in SCW(N)11.20% and PV(N)11.20% sorbents reacted with H_2S to produce MnS. But the binding energies of

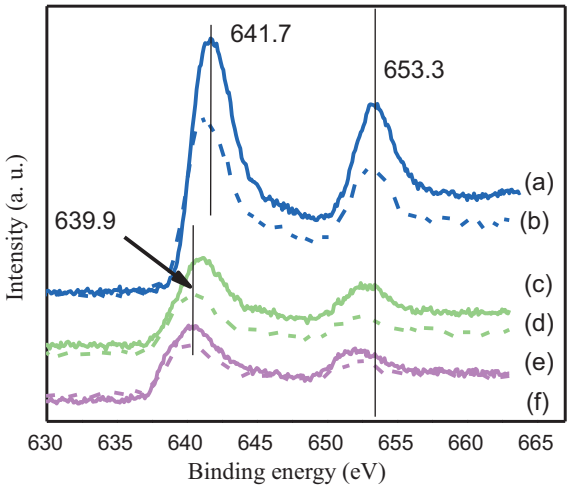

Fig. 6. The XPS spectra of Mn $2p_{3/2}$ of fresh and used sorbents: (a) PV(N)11.2%; (b) S-PV(N)11.2%; (c) SCW(N)11.20%; (d) S-SCW(N)11.20%; (e) SCW(A)11.20%; (f) S-SCW(A)11.20%.

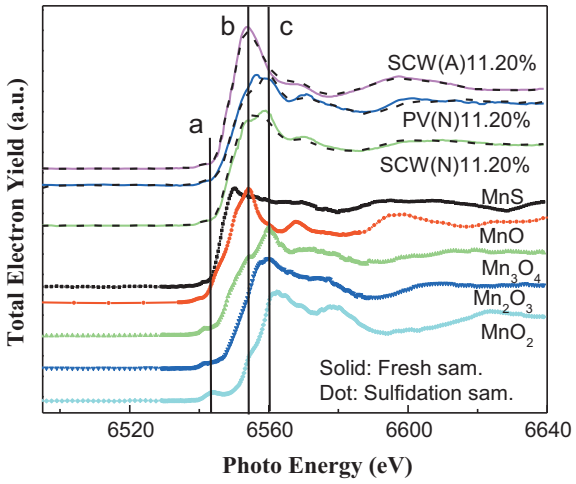

Fig. 7. Mn K-edge XANES spectra of reference and the fresh (solid line) and used sorbents (dot line).

S-SCW(A)11.20% sorbent do not change any more and only the peak intensities increase, which suggests only a little Mn species can react with H_2S and the main form of Mn remains to be Mn_2SiO_4-like species in SCW(A)11.20%.

3.2.5. Mn and S K-edge XANES

In order to understand the forms and changes of Mn in the different samples before and after sulfidation, XAS spectra were recorded and analyzed. Fig. 7 shows the normalized Mn K-edge XANES spectra of reference compounds, the fresh and used sorbents. Mn K-edge spectrum is dominated by transition of Mn 1s electron to the Mn 4p empty orbitals (peak b), with a weak pre-edge peak (peak a) corresponding to the transition of Mn 1s electron to the Mn 3d and ligand up mixed orbitals [42]. The chemical shift of edge jump (peak a) to the higher energy is clearly observed as Mn oxidation state increases from +2 (MnO) to +4 (MnO_2). The results shown in Fig. 8 indicate that the absorption peaks of Mn in the three sorbents are different. For SCW(A)11.20% sample, the main absorption peak appeared at lower energy (6553.9 eV), very close to energy positions of Mn^{2+} reference compounds (MnS and MnO). In fact, the absorption peak of Mn_2SiO_4-like species is reported to be slightly lower than that of MnO [43]. This suggests that Mn in the SCW(A)11.20% exists as Mn^{2+} species, such as Mn_2SiO_4, in agreement with the XRD finding. It should be noted that there is almost no change to the Mn K-edge spectra of SCW(A)11.20% samples before and after sulfidation, thus implying that Mn in SCW(A)11.20% sample has very low activity with H_2S. There are two peaks (peak b at 6554.1 eV and peak c at 6560.1 eV) in the spectrum of SCW(N)11.20% sample [44], while peak c is almost not resolvable in the S-SCW(N)11.20% sample. This coexistence of Mn^{2+} and Mn^{3+} is in agreement with previous studies on Mn incorporation into porous materials [21,44]. It is clear from Fig. 7 that peak c is the characteristic peak of Mn_3O_4, therefore suggesting that the Mn is in the form of Mn_3O_4 in the SCW(N) 11.20%, which is in agreement with XRD and XPS results; and the Mn in the S-SCW(N)11.20% has been partly reduced to Mn^{2+}. For PV(N)11.20%, it appears that Mn is mostly in +3 oxidation state, with some Mn^{2+}, in the form of Mn_2O_3. This is different with XRD results that Mn is in the form MnO in the bulk phase. After sulfidation, the lower energy peak at 6556.1 eV, corresponding to that of Mn_3O_4, decreases in intensity, suggesting the reduction of Mn in S-PV(N)11.20% sample.

The S K-edge XANES spectra of reference compounds (MnS), fresh and used samples are presented in Fig. 8. It can be seen that spectra of all three sorbents are very similar to that of AC, with peaks assigned to sulfide and sulfonic acid sulfur (a: 2473.5 eV and b: 2480.3 eV, respectively) [45,46], suggesting that different preparation methods do not modify S forms. For samples after sulfidation reaction, their S K-edge spectra are significantly different from that of AC. The position of peak a shifted lower to 2471.7 eV, an energy position similar to that of MnS, and peak b shifted to higher energy, characteristic peak of metal sulfate sulfur. It should be noted that peak intensity of MnS in Fig. 8(b) is in the order of S-PV(N)11.20% > S-SCW(N)11.20% > S-SCW(A)11.20%, consistent with the desulfurization performance. The observation of manganese sulfate in samples after sulfidation is not supported partly by the XRD data, but we should note that the TEY at S K-edge is relatively surface sensitive and some of the sulfate could be due to the surface oxidation when the sample was exposed to air before the XAS measurements.

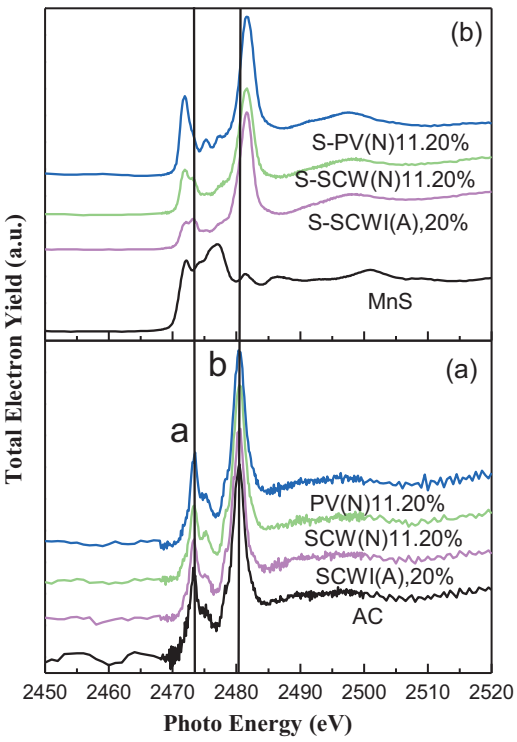

Fig. 8. S K-edge XANES spectra of AC, MnS and samples: (a) fresh sample; (b) used sample.

3.3. The regeneration of the sorbent

From technology point of view, the available sorbents for industry should be low cost, high sulfur capacity and easily regenerated sorbents. In order to know the regeneration ability of the present samples, the regeneration of SCW(N)11.20% was investigated as discussed in Section 2.2. The results of the three desulfurization/regeneration cycle experiments for SCW(N)11.20% are shown in Fig. 9. The SCW(N)11.20% sorbent has a breakthrough time of 600 min and a sulfur capacity of 3.78 g S/100 g sorbent after the first regeneration, vs. 640 min and 3.91 g S/100 g sorbent for the fresh sample. The performance of SCW(N)11.20% is decreased smoothly after the second and third regenerations. Although its efficiency in removing H_2S is slightly worse than that of the fresh sorbent, the SCW(N)11.20% still maintains good heat stability during the three desulfurization/regeneration cycles at the desulfurization temperature of 350 °C. The results show that the Mn/AC is a regenerable sorbent for removing H_2S from hot coal gas. In the future, more tests of the desulfurization/regeneration cycle will be performed to compare different sorbents prepared by different methods.

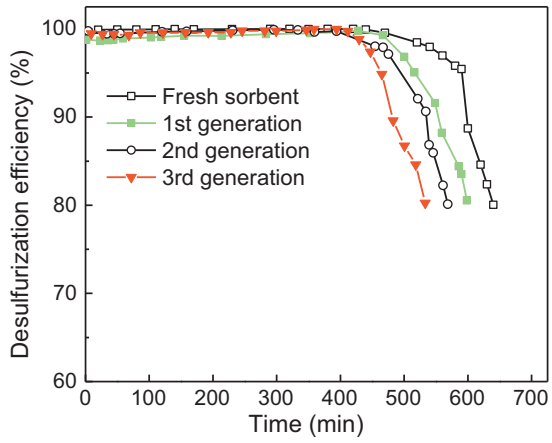

Fig. 9. Desulfurization efficiency of SCW(N)11.20% sorbents in three desulfurization/regeneration cycles.

4. Conclusions

The sorbents for removing H_2S from hot coal gas were prepared using SCWI and PVI methods with different precursor solutions. The XRD, SEM, TEM, XPS and XAS techniques were employed to characterize the fresh and used sorbents. It is found that the preparation methods and precursor solutions influence the dispersion, particle sizes and the chemical states of the active components in the sorbents, which are the dominant parameters influencing their desulfurization activity.

The SCW(N) sorbents show better sulfidation performance than the SCW(A) sorbents. This is because the active phase of the SCW(N) sorbents is Mn_3O_4, which is well dispersed on AC support, while the seriously aggregated and poor activity mixture of Mn_2SiO_4-like species form on AC support in the SCW(A) sorbents. Mn_2SiO_4-like species has no desulfurization activity and leads to the poorer sulfidation performance of SCW(A) sorbents than that of the SCW(N) sorbents.

Mn^{2+} and Mn^{3+} in the prepared sorbents are favorable for the sulfidation reaction. For the sorbents with 2.80 and 5.60% manganese precursor, SCW(N) has better dispersed Mn active species than the PV(N) sorbents, which results in the better sulfidation performance of the SCW(N) sorbents than that of the PV(N) sorbents. So, the superiority of SCW(N) prepared at lower Mn concentration is used for real catalytic reaction (such as the above mentioned) will be more distinct compared to the catalyst prepared by the traditional method than the adsorption reaction for the removal of H_2S. But, as the Mn content of the precursor is increased to 11.20%, the metal oxide particles on AC support is seriously aggregated and results in less active Mn sites of the sorbents, which leads to poorer sulfidation performance of the SCW(N)11.20% sorbent than that of the PV(N)11.20% sorbent.

Acknowledgments

This work was supported by the National Natural Science Foundation of China (20976117, 21006067), the National Basic Research Program of China (2012CB723105), the Shanxi Province Natural Science Foundation (2011021008-4 and 2010021008-1), and China Postdoctoral Science Foundation (CPSF, 20110491630). We also thank the CLS staff for the technical support. The CLS is financially supported by NSERC Canada, CIHR, NRC and the University of Saskatchewan.

References

[1] J.H. Swisher, K. Schwerdtfeger, Review of metals and binary oxides as sorbents for removing sulfur from coal-derived gases, J. Mater. Eng. Perform. 1 (1992) 399–408.
[2] K.A. Brenneman, R.A. James, E.A. Gross, D.C. Dorman, Olfactory neuron loss in adult male CD rats following subchronic inhalation exposure to hydrogen sulfide, Toxicol. Pathol. 28 (2000) 326–333.
[3] R.B. Slimane, J. Abbasian, Regenerable mixed metal oxide sorbents for coal gas desulfurization at moderate temperatures, Adv. Environ. Res. 4 (2000) 147–162.
[4] H.L. Fan, Y.X. Li, C.H. Li, H.X. Guo, K.C. Xie, The apparent kinetics of H_2S removal by zinc oxide in the presence of hydrogen, Fuel 81 (2002) 91–96.
[5] X.R. Ren, L.P. Chang, F. Li, K.C. Xie, Study of intrinsic sulfidation behavior of Fe_2O_3 for high temperature H_2S removal, Fuel 89 (2010) 883–887.
[6] J. Abbasian, R.B. Slimane, A regenerable copper-based sorbent for H_2S removal from coal gases, Ind. Eng. Chem. Res. 37 (1998) 2775–2782.
[7] P. Yrjas, K. Iisa, M. Hupa, Limestone and dolomite as sulfur absorbents under pressurized gasification conditions, Fuel 75 (1996) 89–95.
[8] G.D. Focht, P.V. Ranade, D.P. Harrison, High-temperature desulfurization using zinc ferrite-reduction and sulfidation kinetics, Chem. Eng. Sci. 43 (1988) 3005–3013.
[9] S. Lew, A.F. Sarofim, M. Flytzani-Stephanopoulos, The reduction of zinc titanate and zinc-oxide solids, Chem. Eng. Sci. 47 (1992) 1421–1431.
[10] H. Atakül, J.P. Wakker, A.W. Gerritsen, P.J. van den Berg, Removal of H_2S from fuel gases at high-temperatures using MnO/gamma-Al_2O_3, Fuel 74 (1995) 187–191.
[11] S. Valdés-Solis, G. Marbán, A.B. Fuertes, Low-temperature SCR of NOx with NH_3 over carbon-ceramic supported catalysts, Appl. Catal. B 46 (2003) 261–271.
[12] E. García-Bordejé, M.J. Lázaro, R. Moliner, J.F. Galindo, J. Sotres, A.M. Baró, Structure of vanadium oxide supported on mesoporous carbon-coated monoliths and relationship with its catalytic performance in the SCR of NO at low temperatures, J. Catal. 223 (2004) 395–403.
[13] V.R. Choudhary, P.A. Chaudhari, V.S. Narkhede, Solvent-free liquid phase oxidation of benzyl alcohol to benzaldehyde by molecular oxygen using non-noble transition metal containing hydrotalcite-like solid catalysts, Catal. Commun. 4 (2003) 171–175.
[14] Y. Su, L.-C. Wang, Y.-M. Liu, Y. Cao, H.-Y. He, K.-N. Fan, Microwave-accelerated solvent-free aerobic oxidation of benzyl alcohol over efficient and reusable manganese oxides, Catal. Commun. 8 (2007) 2181–2185.
[15] J.P. Wakker, A.W. Gerritsen, J.A. Moulijn, High temperature hydrogen sulfide and carbonyl sulfide removal with manganese oxide (MnO) and iron oxide (FeO) on.gamma.-alumina acceptors, Ind. Eng. Chem. Res. 32 (1993) 139–149.
[16] W.J.W. Bakker, F. Kapteijn, J.A. Moulijn, A high capacity manganese-based sorbent for regenerative high temperature desulfurization with direct sulfur production: conceptual process application to coal gas cleaning, Chem. Eng. J. 96 (2003) 223–235.
[17] H. Atakül, J.P. Wakker, A.W. Gerritsen, P.J. van den Berg, Regeneration of MnO/[gamma]-Al_2O_3 used for high-temperature desulfurization of fuel gases, Fuel 75 (1996) 373–378.
[18] Y. Ma, S.G. Wang, M.H. Fan, W.X. Gong, B.Y. Gao, Characteristics and defluoridation performance of granular activated carbons coated with manganese oxides, J. Hazard. Mater. 168 (2009) 1140–1146.
[19] F. Kapteijn, A.D. Vanlangeveld, J.A. Moulijn, A. Andreini, M.A. Vuurman, A.M. Turek, J.M. Jehng, I.E. Wachs, Alumina-supported manganese oxide catalysts. 1. Characterization-effect of precursor and loading, J. Catal. 150 (1994) 94–104.
[20] F. Kapteijn, L. Singoredjo, M. Vandriel, A. Andreini, J.A. Moulijn, G. Ramis, G. Busca, Alumina-supported manganese oxide catalysts. 2. Surface characterization and adsorption of ammonia and nitric-oxide, J. Catal. 150 (1994) 105–116.
[21] Q.H. Tang, X.N. Huang, Y.T. Chen, T. Liu, Y.H. Yang, Characterization, catalytic application of highly dispersed manganese oxides supported on activated carbon, J. Mol. Catal. A: Chem. 301 (2009) 24–30.
[22] R. Viswanathan, G.D. Lilly, W.F. Gale, R.B. Gupta, Formation of zinc oxide–titanium dioxide composite nanoparticles in supercritical water, Ind. Eng. Chem. Res. 42 (2003) 5535–5540.
[23] Y. Hakuta, H. Hayashi, K. Arai, Fine particle formation using supercritical fluids, Curr. Opin. Solid State Mater. Sci. 7 (2003) 341–351.
[24] K. Byrappa, T. Adschiri, Hydrothermal technology for nanotechnology, Prog. Cryst. Growth Charact. Mater. 53 (2007) 117–166.
[25] A. Aimable, H. Muhr, C. Gentric, F. Bernard, F. Le Cras, D. Aymes, Continuous hydrothermal synthesis of inorganic nanopowders in supercritical water: towards a better control of the process, Powder Technol. 190 (2009) 99–106.
[26] P.A. Marrone, G.T. Hong, M.H. Spritzer, Developments in supercritical water as a medium for oxidation reforming, and synthesis, J. Adv. Oxid. Technol. 10 (2007) 157–168.
[27] E. Reverchon, R. Adami, Nanomaterials and supercritical fluids, J. Supercrit. Fluids 37 (2006) 1–22.
[28] J. Otsu, Y. Oshima, New approaches to the preparation of metal or metal oxide particles on the surface of porous materials using supercritical water: development of supercritical water impregnation method, J. Supercrit. Fluids 33 (2005) 61–67.
[29] O. Sawai, Y. Oshima, Mechanism of silver nano-particles formation on alpha-alumina using supercritical water, J. Mater. Sci. 43 (2008) 2293–2299.
[30] C.B. Xu, A.S. Teja, Supercritical water synthesis and deposition of iron oxide (alpha-Fe_2O_3) nanoparticles in activated carbon, J. Supercrit. Fluids 39 (2006) 135–141.

[31] C.B. Xu, A.S. Teja, Characteristics of iron oxide/activated carbon nanocomposites prepared using supercritical water, Appl. Catal. A 348 (2008) 251–256.
[32] B. Qiu, L.N. Han, J.C. Wang, L.P. Chang, W.R. Bao, Preparation of sorbents loaded on activated carbon to remove H_2S from hot coal gas by supercritical water Impregnation, Energy Fuels 25 (2011) 591–595.
[33] X. Zheng, W. Bao, Q. Jin, L. Chang, K. Xie, Use of high-pressure impregnation in preparing Zn-based sorbents for deep desulfurization of hot coal gas, Energy Fuels 25 (2011) 2997–3001.
[34] Y.F. Hu, D. Chevrier, G. Wright, R. Igarashi, A. Sitnikov, Preliminary commissioning and performance of the soft X-ray micro-characterization beamline at the Canadian light source, AIP Proc. 1234 (2010) 343–346.
[35] K.S.W. Sing, D.H.E.A.W. Haul, L. Moscou, R.A. Pierotti, J. Rouquerol, T. Siemieniewska, Reporting physisorption data for gas/solid systems with special reference to the determination of surface area and porosity, Pure Appl. Chem. 57 (1985) 603–620.
[36] M.I. Zaki, A.K.H. Nohman, G.A.M. Hussein, Y.E. Nashed, Composition, structure and surface acid–base behaviour of manganese oxide dispersed on silica, Colloids Surf. A 99 (1995) 247–253.
[37] Y. Kim, M. Shin, C. Tang, J. Lee, Wettability of $Mn_xSi_yO_z$ by liquid Zn–Al alloys, Metall. Mater. Trans. B 41 (2010) 872–875.
[38] S. Lew, A.F. Sarofim, M. Flytzani-Stephanopoulos, Sulfidation of zinc titanate and zinc oxide solids, Ind. Eng. Chem. Res. 31 (1992) 1890–1899.
[39] D. Choi, J. Lee, S. Jang, B. Ahn, D. Choi, Adsorption dynamics of hydrogen sulfide in impregnated activated carbon bed, Adsorption 14 (2008) 533–538.
[40] K. Polychronopoulou, F. Cabello Galisteo, M. López Granados, J.L.G. Fierro, T. Bakas, A.M. Efstathiou, Novel Fe–Mn–Zn–Ti–O mixed-metal oxides for the low-temperature removal of H_2S from gas streams in the presence of H_2, CO_2, and H_2O, J. Catal. 236 (2005) 205–220.
[41] X. Vanden Eynde, J.P. Servais, M. Lamberigts, Investigation into the surface selective oxidation of dual-phase steels by XPS, SAM and SIMS, Surf. Interface Anal. 35 (2003) 1004–1014.
[42] F. Farges, Ab initio and experimental pre-edge investigations of the Mn K-edge XANES in oxide-type materials, Phys. Rev. B 71 (2005) 155109.
[43] D.A. McKeown, W.K. Kot, H. Gan, I.L. Pegg, X-ray absorption studies of manganese valence and local environment in borosilicate waste glasses, J. Non-Cryst. Solids 328 (2003) 71–89.
[44] N.N. Tušar, D. Maučec, M. Rangus, I. Arčon, M. Mazaj, M. Cotman, A. Pintar, V. Kaučič, Manganese functionalized silicate nanoparticles as a fenton-type catalyst for water purification by advanced oxidation processes (AOP), Adv. Funct. Mater. (2011), doi:10.1002/adfm.201102361.
[45] M.E. Fleet, XANES spectroscopy of sulfur in earth materials, Can. Mineral. 43 (2005) 1811–1838.
[46] K.A. Evans, H.S.C. O'Neill, J.A. Mavrogenes, N.S. Keller, L.Y. Jang, J.F. Lee, XANES evidence for sulphur speciation in Mn-, Ni- and W-bearing silicate melts, Geochim. Cosmochim. Acta 73 (2009) 6847–6867.